# On the Applicability of SISO and MIMO Impedance-Based Stability Assessment of DC–DC Interlinking Converters

Ružica Cvetanović, *Graduate Student Member, IEEE*, Ivan Z. Petrić, *Member, IEEE*, Paolo Mattavelli, *Fellow, IEEE*, and Simone Buso, *Member, IEEE*

***Abstract*—This article presents a formal mathematical correlation between the standardly used *port-level* (terminated) single-input single-output (SISO), and the recently acknowledged *device-level* (unterminated) multiple-input multiple-output (MIMO) impedance-based method for the stability assessment of dc–dc interlinking converters. Based on this, the conditions that must be met to ensure the correct stability assessment by the SISO method applied to a single port-pair are derived. It is shown that without prior knowledge on whether these conditions are met, the SISO method must be applied to every port-pair to account for possible *port-level hidden dynamics*. Alternatively, the MIMO method can be used, which is revealed to inherently account for any *port-level hidden dynamics*. It is further analyzed which method is advantageous in terms of computational complexity, intuitiveness, and simplicity for applications featuring meshed grids or multiport interlinking converters, as well as in terms of interpreting the resulting stability margins. Finally, suitability of the MIMO method for termination-independent stability-oriented controller design and stability assessment based on measurements is highlighted. The presented methodology is illustrated for a simplified dc system with a current-controlled buck converter. Analytical stability predictions are validated using hardware-in-the-loop simulations and also experimentally, using a laboratory hardware prototype.**

***Index Terms*—Impedance-based stability analysis, interlinking multiport dc–dc converters, (meshed) power electronics grids port-coupling, port-level hidden dynamics.**

## I. Introduction

POWER electronics-dominated systems are becoming prevalent in various industrial, residential, and transportation applications [1], [2], [3], [4]. Although they enable efficient integration of various renewable energy sources, electronically controlled loads, and storage devices [1], their stability is of great concern [2], [5]. For evaluating small-signal stability properties of such systems, an impedance-based stability assessment is typically performed at a certain port (point of connection) [2], [4], [5], [6], [7], [8], [9], [10], [11], [12], [13], [14]. The subsystems seen at each side of that port are represented by the corresponding Northon/Thevenin equivalent circuits and the (inverse) Nyquist criterion (NC) is applied to the so-called minor-loop gain, defined as the product/ratio of the corresponding, *terminated* [2], [6], [7] impedances/admittances (jointly referred to as immittances [9]). This *port-level* impedance-based method is hereafter also referred to as the single-input single-output (SISO) one. Although widely used in the literature [2], [4], [5], [6], [7], [8], [9], [10], [11], [12], [13], [14], when applied to a single port only, this method may lead to a wrong prediction of stability [5], [8]. This occurs when at the considered port the system features *unstable port-level hidden dynamics*, i.e., when the unstable poles do not appear in the transfer functions corresponding to that port [15]. Some examples of this are reported in [5], [8], [16], and [17] for radial (nonmeshed) systems. Along the line of *unstable port-level hidden dynamics*, further limitations of the *port-level* impedance-based method may arise when, to enhance reliability and flexibility, instead of radial, the system features a meshed structure [8], [18]. Moreover, for such systems, even in absence of any *unstable port-level hidden dynamics*, this method loses intuitiveness as the definition of the terminated immittances provides little physical insight when the ports are fully coupled.

As a more general method, the *device-level* impedance-based method can be used, which is hereafter also referred to as multiple-input multiple-output (MIMO) one. The method relies on the *all-port unterminated* MIMO representation [6], [19], [20], [21], [22], [23] of both subsystems of interest: the converter under study and the rest of the system it interconnects. The subsystems' immittances within the Norton/Thevenin equivalents are in this case transfer function matrices, and the generalized Nyquist criterion (GNC) [24], [25] is applied to the resulting MIMO minor loop gain. Other than briefly outlining the idea in [26] and [27], the application of such MIMO impedance-based method, to the best of authors' knowledge, has not been thoroughly analyzed for dc systems. As for ac systems, a variant of the MIMO impedance-based method that additionally involves the passive/active component grouping

Manuscript received 18 December 2023; revised 19 March 2024; accepted 13 May 2024. Date of publication 20 May 2024; date of current version 16 July 2024. This work was supported by the European Union's Horizon Europe research and innovation program in the framework of the project "iPLUG" under Grant 101069770. Recommended for publication by Associate Editor M. Saeedifard. *(Corresponding author: Ružica Cvetanović.)*

Ružica Cvetanović and Simone Buso are with the Department of Information Engineering, University of Padova, 35131 Padova, Italy (e-mail: ruzica.cvetanovic@phd.unipd.it; simone.buso@dei.unipd.it).

Ivan Z. Petrić is with the Hanwha Q CELLS America Inc., Santa Clara, CA92618 USA (e-mail: ivan.petric@phd.unipd.it).

Paolo Mattavelli is with the Department of Management and Engineering, University of Padova, 36100 Vicenza, Italy (e-mail: paolo.mattavelli@unipd.it).

Color versions of one or more figures in this article are available at https://doi.org/10.1109/TPEL.2024.3403236.

Digital Object Identifier 10.1109/TPEL.2024.3403236

was used in [21], [22], and [23], to avoid appearance of the termination-caused right half plane (RHP) poles in the minor loop gain. Nevertheless, application of the *device-level* MIMO method in light of accounting for the *port-level hidden dynamics*, which, as mentioned above, may be disregarded by the *port-level* impedance-based method, has not been previously explored. In addition, the potential of the *device-level* method to handle meshed systems and/or systems with multiport converters has not been discussed either. Finally, its relationship with the *port-level* impedance-based method has not been derived so far.

To fill in these gaps, this article presents a formal mathematical correlation between the standardly used SISO, and the recently acknowledged MIMO impedance-based method for stability assessment of dc–dc interlinking converters. Based on this, the conditions under which the methods account for the *(unstable) port-level hidden dynamics* are for the first time derived and the computational complexity required for this is discussed. It is revealed that the MIMO method is advantageous in these aspects. Furthermore, the suitability of the SISO and the MIMO methods for stability assessment in systems with meshed structures and/or multiport converters, as well as for defining various stability margins is explored. Finally, the unterminated (black-box) representation-related assets of the MIMO method are underlined, which are relevant when the stability analysis is to be performed based on measurements, rather than analytical models, as well as when robust termination-independent stabilization methods are to be developed.

The rest of this article is organized as follows. Section II explains unterminated small-signal modeling and the MIMO impedance-based method. Section III recalls different loop-gain-based approaches for determining stability of a MIMO feedback system and provides relationship between the MIMO and the SISO impedance-based methods. Section IV illustrates the use of the presented methodology on a simplified dc system, where a current-controlled buck converter is used as an interlinking converter. Hardware-in-the-loop (HIL) and experimental validations are also presented. Advantages and disadvantages of the MIMO and the SISO impedance-based method are summarized in Section V. Section VI concludes this article.

## II. Impedance-Based Stability Assessment

### A. System Under Study

This article considers dc power electronic systems, such as the one illustrated in Fig. 1(a). It features an interlinking (intermediate-bus) dc–dc converter, encircled in red in Fig. 1(a). For the purpose of keeping the presentation clear, the considered converter has only two ports. Nevertheless, the analysis is applicable to multiport interlinking converters as well. The proposed methodology also accounts for the case when, in parallel to the considered interlinking converter, additional interlinking converters exist, such as one shown in gray in Fig. 1(a), or when instead of radial, the network features meshed configuration. Since in either of these cases the ports of the converter under study are not solely interconnected by the converter itself, but also by other components of the system, such structure is referred to as a meshed system/grid.

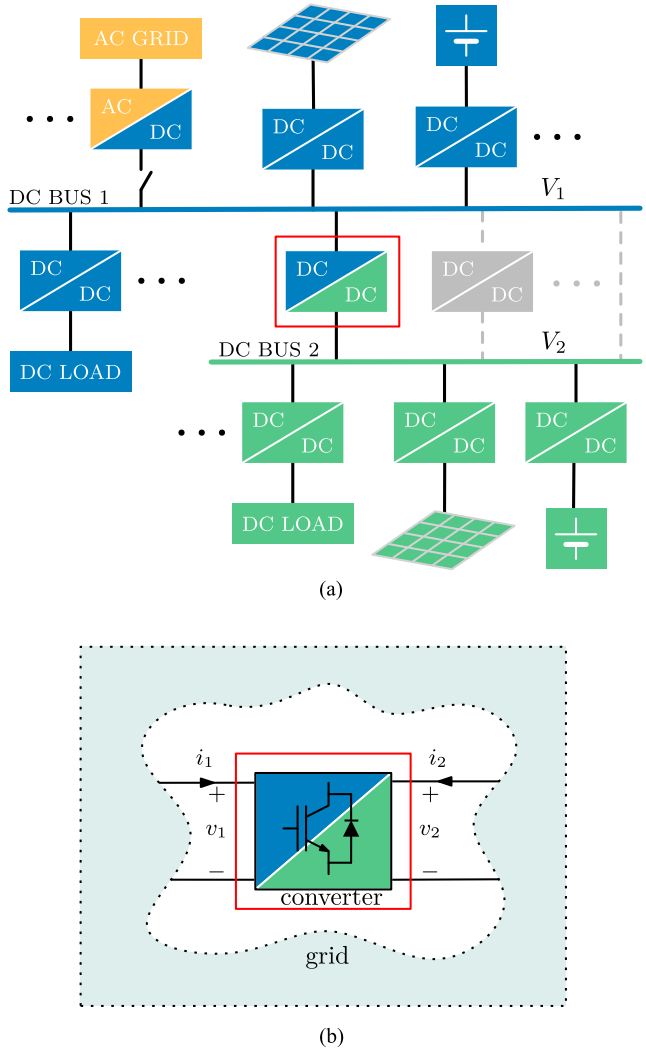


Fig. 1. (a) DC power electronic system under study. The DC–DC converter in gray illustrates the possibility of forming a meshed system structure. (b) The two-subsystem equivalent representation, featuring the grid and the two-port interlinking DC-DC converter, encircled in red.

The goal of the sections that follow is to present a general impedance-based method for determining small-signal stability properties of an interlinking converter, such as the one from Fig. 1(a). For this, the system is first split into two-subsystems: the converter and the grid, as shown in Fig. 1(b). The subsystems are then represented by their small-signal Norton/Thevenin equivalent circuits, and the properties of the resulting impedance/admittance network are used to determine the small-signal stability of the interconnected system.

### B. Small-Signal Representation

In this article, the Norton equivalent small-signal $s$-domain representation is used for the converter, while the Thevenin one is used for the grid.[1] This representation is shown in Fig. 2,

[1]Discussion about which equivalent representation of each of the subsystems should be used to avoid appearance of the RHP poles in the minor-loop gain is out of the scope of this article [7], [21], [28].

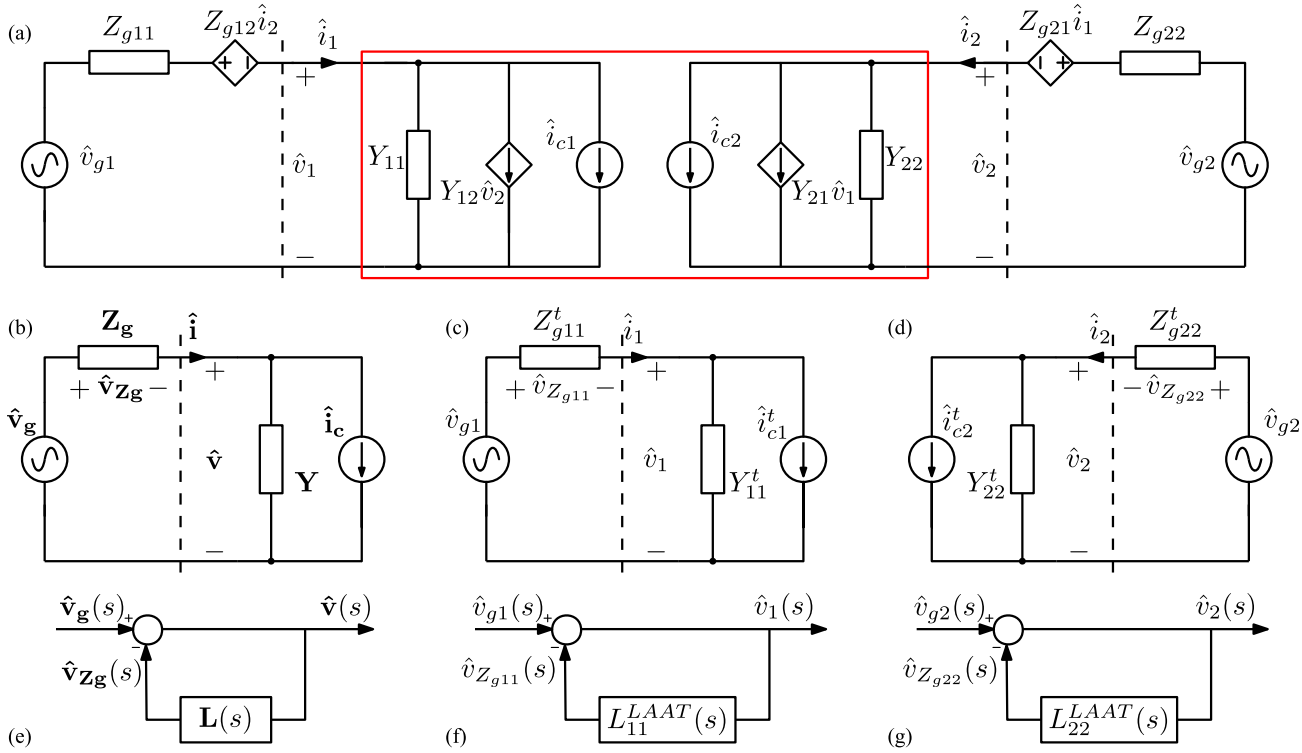


Fig. 2. Small-signal representation of the system from Fig. 1, featuring: (a) unterminated two-port representation of the converter and the grid; (b)–(d) the simplified Norton/Thevenin equivalent representation used for (b) the MIMO impedance-based stability assessment and for the SISO impedance-based stability assessment at (c) port 1 (port-pair (1,1)) and (d) at port 2 (port-pair (2,2)); (e)–(g) the equivalent feedback system corresponding to (b)–(d) with $\mathbf{i_c} = 0$, $i^t_{c1} = 0$, and $i^t_{c2} = 0$.

where $\hat{}$ is used to denote the corresponding small-signal perturbation components of the quantities from Fig. 1(b). The Norton/Thevenin equivalents are determined considering the MIMO nature of the system, which relies on the unterminated modeling approach [19]. Along this line, the converter is represented via the Norton current sources $\hat{i}_{c1}(s)$ and $\hat{i}_{c2}(s)$ (that model the converter's response to reference perturbation), and the unterminated MIMO admittance matrix[2] $\mathbf{Y}(s)$

$$\mathbf{Y(s)} = \begin{bmatrix} Y_{11}(s) & Y_{12}(s) \\ Y_{21}(s) & Y_{22}(s) \end{bmatrix} \tag{1}$$

where $s$ is the complex variable of the Laplace transform, and

$$Y_{11}(s) = \left.\frac{\hat{i}_1(s)}{\hat{v}_1(s)}\right|_{\hat{v}_2(s)=0,\hat{i}_{c1}(s)=0},$$

$$Y_{22}(s) = \left.\frac{\hat{i}_2(s)}{\hat{v}_2(s)}\right|_{\hat{v}_1(s)=0,\hat{i}_{c2}(s)=0},$$

$$Y_{12}(s) = \left.\frac{\hat{i}_1(s)}{\hat{v}_2(s)}\right|_{\hat{v}_1(s)=0,\hat{i}_{c1}(s)=0},$$

$$Y_{21}(s) = \left.\frac{\hat{i}_2(s)}{\hat{v}_1(s)}\right|_{\hat{v}_2(s)=0,\hat{i}_{c2}(s)=0}. \tag{2}$$

For a given converter topology and control system structure, the expressions for $Y_{11}(s)$, $Y_{12}(s)$, $Y_{21}(s)$, and $Y_{22}(s)$ can be derived based on the small-signal model of the converter and its control system [26], [29].

Similarly, the grid is represented by the Thevenin voltage sources $\hat{v}_{g1}(s)$ and $\hat{v}_{g2}(s)$, and the unterminated MIMO impedance matrix $\mathbf{Z_g}(s)$

$$\mathbf{Z_g}(s) = \begin{bmatrix} Z_{g11}(s) & Z_{g12}(s) \\ Z_{g21}(s) & Z_{g22}(s) \end{bmatrix}, \tag{3}$$

where $Z_{g11}$, $Z_{g12}$, $Z_{g21}$, and $Z_{g22}$ are defined analogously to $Y_{11}$, $Y_{12}$, $Y_{21}$, and $Y_{22}$ in (2). In case the system is not meshed, i.e., the two buses are interconnected only via the considered converter, the grid impedance matrix becomes diagonal

$$\mathbf{Z_g}(s) = \begin{bmatrix} Z_{g11}(s) & 0 \\ 0 & Z_{g22}(s) \end{bmatrix}. \tag{4}$$

### C. Device-Level (MIMO) Impedance-Based Method

As a general method for assessing stability of an interlinking converter, such as the one from Fig. 1(b), the MIMO impedance-based method can be used, as explained as follows. According

[2]In this article, a bold notation is used for matrices and vectors, while an italic one is used for scalars.

to Fig. 2(a), the following holds:

$$\hat{\mathbf{v}}(s)|_{\hat{\mathbf{i}}_\mathbf{c}(s)=0} = \left(\mathbf{I}+\mathbf{Y}(s)\mathbf{Z}_\mathbf{g}(s)\right)^{-1}\hat{\mathbf{v}}_\mathbf{g}(s) \tag{5}$$

$$\hat{\mathbf{i}}(s)|_{\hat{\mathbf{v}}_\mathbf{g}(s)=0} = \left(\mathbf{I}+\mathbf{Y}(s)\mathbf{Z}_\mathbf{g}(s)\right)^{-1}\hat{\mathbf{i}}_\mathbf{c}(s) \tag{6}$$

where $\mathbf{I}$ is the identity matrix, $\hat{\mathbf{v}}(s)=[\hat{v}_1(s),\hat{v}_2(s)]^T$, $\hat{\mathbf{v}}_\mathbf{g}(s)=[\hat{v}_{g1}(s),\hat{v}_{g2}(s)]^T$, $\hat{\mathbf{i}}_\mathbf{c}(s)=[\hat{i}_{c1}(s),\hat{i}_{c2}(s)]^T$ and $T$ is the transpose operator. Subsequently, the circuit from Fig. 2(a) can be represented in a compact form shown in Fig. 2(b). Then, assuming that the grid and the converter are standalone stable ($\hat{\mathbf{i}}_\mathbf{c}(s)$ and $\hat{\mathbf{v}}_\mathbf{g}(s)$ are stable), stability of the interconnected system is determined by the stability of the MIMO closed-loop system from Fig. 2(e), where

$$\mathbf{L}(s)=\mathbf{Y}(s)\mathbf{Z}_\mathbf{g}(s)=\begin{bmatrix}L_{11}(s) & L_{12}(s)\\ L_{21}(s) & L_{22}(s)\end{bmatrix} \tag{7}$$

is the corresponding (minor) loop gain. Consequently, as explained in Section III-A, the generalized NC [25], [24] can be applied to (7) and used to determine stability of the interconnected system. This and alternative approaches for determining the system stability are discussed in the following section.

## III. Loop-Gain-Based Stability Assessment of a MIMO Feedback System

With the goal of providing a correlation between the MIMO and the SISO impedance-based methods, this section first recalls different loop-gain-based approaches for determining the stability of a linear time-invariant MIMO feedback system $\Sigma_T$, such as the one from Fig. 2(e). Its loop-gain transfer function matrix $\mathbf{L}(s)$ is given by (7), while the corresponding closed-loop transfer function matrix (from $\mathbf{v}_\mathbf{g}(s)$ to $\mathbf{v}(s)$, which, according to (5) and (6), is the same as the transfer function matrix from $\mathbf{i}_\mathbf{c}(s)$ to $\mathbf{i}(s)$) is given by

$$\mathbf{T}(s)=\left(\mathbf{I}+\mathbf{L}(s)\right)^{-1}=\begin{bmatrix}T_{11}(s) & T_{12}(s)\\ T_{21}(s) & T_{22}(s)\end{bmatrix} \tag{8}$$

where

$$T_{11}(s)=\frac{L_{22}(s)+1}{\det(\mathbf{I}+\mathbf{L}(s))},\ T_{12}(s)=-\frac{L_{12}(s)}{\det(\mathbf{I}+\mathbf{L}(s))}$$
$$T_{21}(s)=-\frac{L_{21}(s)}{\det(\mathbf{I}+\mathbf{L}(s))},\ T_{22}(s)=\frac{L_{11}(s)+1}{\det(\mathbf{I}+\mathbf{L}(s))}. \tag{9}$$

As any transfer function-based methodology, the subsequent analysis can, in a general case, be used only to determine the bounded-input bounded-output (BIBO) stability [24], [30] of the considered MIMO system $\Sigma_T$. However, BIBO stability may not be sufficient to ensure internal stability, if $\Sigma_T$ is not observable or not controllable [24], [30]. Nevertheless, if $\Sigma_T$ is detectable and stabilizable, its internal stability is equivalent to its BIBO stability [24], [30]. Hence, stability assessment of the MIMO transfer function matrix $\mathbf{T}(s)$ is valid for determining also the internal stability of $\Sigma_T$, as long as the below stated Condition 1 is satisfied, which is assumed in this article.

*Condition 1:* A state-space representation of the considered MIMO system $\Sigma_T$ (which corresponds to $\mathbf{T}(s)$ from (8)) features no unobservable or uncontrollable modes (eigenvalues) in the RHP, i.e., $\Sigma_T$ is detectable and stabilizable (it features no *unstable device-level hidden dynamics*).[3]

### A. MIMO Loop-Gain-Based Approach

The first stability assessment approach to be recalled is based on the MIMO loop-gain and is stated as follows.

*Approach 1:* Stability of the closed-loop MIMO system $\mathbf{T}(s)$ from (8) and Fig. 2(e) can be determined by applying the GNC to the corresponding loop-gain transfer function matrix $\mathbf{L}(s)$ from (7) [24].

For this, either the determinant-based GNC or the eigenloci-based GNC can be used [24], [25]. Determinant-based GNC involves applying the NC to

$$L_m(s)=\det(\mathbf{I}+\mathbf{L}(s))-1 \tag{10}$$

and, with $L_m$ being a scalar value, always relies on a single Nyquist plot (NP) [24]. On the other hand, the eigenloci-based GNC involves applying NC to all eigenloci (also called characteristic loci) $\lambda_i$, which are the eigenvalues of $\mathbf{L}(s)$ obtained from $\det(\lambda_i(s)\mathbf{I}-\mathbf{L}(s))=0$ [24], [25]. In this case, the number of the required NPs is equal to the number of systems inputs $N$, which for the system from Fig. 2(a) is equal to two. Note that, since $\det(\mathbf{I}+\mathbf{L}(s))=1+\prod_i\lambda_i(s)$, the determinant-based GNC and the eigenloci-based GNC are equivalent in terms of evaluating whether the system is stable or not. However, they yield *different stability margins*, which brings ambiguity in assessing the system's robustness [24], [31]. Finally, it should be emphasized that, as long as Condition 1 is satisfied, *Approach 1* is always valid for determining internal stability, i.e., its applicability is not conditioned by other properties of the system under study.

### B. SISO Loop-Gain(s)-Based Approach

The second stability assessment approach to be recalled is based on SISO loop-gains and is stated as follows:

*Approach 2a:* Stability of the closed-loop MIMO system $\mathbf{T}(s)$ from (8) and Fig. 2(e) can be determined by applying the NC to *every* loop-at-a-time (LAAT) loop-gain transfer-function [24], [30], [32]

$$L_{ij}^{\text{LAAT}}(s)=\frac{1}{T_{ij}(s)}-1 \tag{11}$$

where, $i,j\in\{1,2,\ldots,N\}$ and, according to (9)

$$L_{11}^{\text{LAAT}}(s)=L_{11}(s)-\frac{L_{12}(s)L_{21}(s)}{1+L_{22}(s)}$$
$$L_{22}^{\text{LAAT}}(s)=L_{22}(s)-\frac{L_{12}(s)L_{21}(s)}{1+L_{11}(s)}$$

[3]Clarification of observability, controllablity, detectability, and stabilizability, along with some examples of systems featuring these properties, is provided in the Appendix.

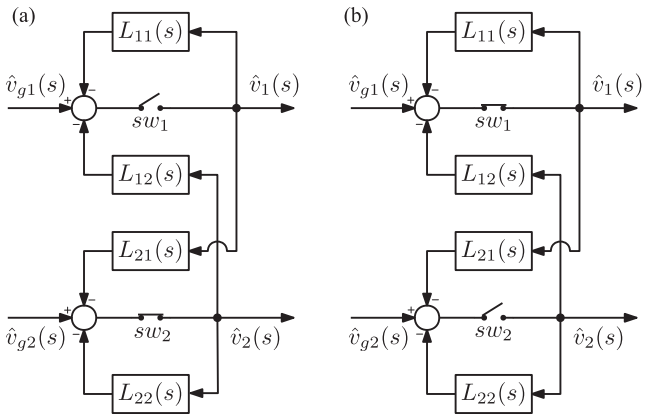


Fig. 3. LAAT representation of the MIMO ($N = 2$) feedback system from Fig. 2(e), obtained by breaking (a) only the loop from the first input $\hat{v}_{g1}$ to the first output $\hat{v}_1$ ($\text{sw}_1$ is open and $\text{sw}_2$ is closed); (b) only the loop from the second input $\hat{v}_{g2}$ to the second output $\hat{v}_2$ ($\text{sw}_1$ is closed and $\text{sw}_2$ is open). The corresponding LAAT SISO loop gains $L_{11}^{\text{LAAT}}(s)$ and $L_{22}^{\text{LAAT}}(s)$ can be obtained from (a) and (b), respectively. Though less intuitive, similar representation can be made for obtaining $L_{12}^{\text{LAAT}}(s)$ and $L_{21}^{\text{LAAT}}(s)$.

$$L_{12}^{\text{LAAT}}(s) = L_{21}(s) - 1 - \frac{(1 + L_{11}(s))(1 + L_{22}(s))}{L_{12}(s)}$$

$$L_{21}^{\text{LAAT}}(s) = L_{12}(s) - 1 - \frac{(1 + L_{11}(s))(1 + L_{22}(s))}{L_{21}(s)}.$$

The idea behind this approach relies on breaking, one at a time, the SISO loops (paths from a single input to the single output) within the MIMO closed-loop system [32], as illustrated in Fig. 3. Stability of the closed-loop SISO system corresponding to the broken loop is then checked by evaluating its loop-gain [32]. By repeating evaluation of *every* SISO loop-gain obtained in this way, stability of the closed-loop MIMO system can be determined. Given that the number of these SISO loop-gains $L_{ij}^{\text{LAAT}}(s)$ is $N^2$, *Approach 2a* relies on $N^2$ NPs. This approach can be simplified to using a single $L_{ij}^{\text{LAAT}}(s)$ in case the Condition 2, stated as follows, is satisfied.

*Condition 2:* A state-space representation of the SISO system $\Sigma_{T_{ij}}$ [which corresponds to $T_{ij}(s)$ in (8) and (9)] features no unobservable or uncontrollable modes (eigenvalues) in the RHP, i.e., $\Sigma_{T_{ij}}$ is detectable and stabilizable. In this case, the MIMO system $\Sigma_T$ is detectable and stabilizable for the SISO variation,[4] i.e., port-pair $(i, j)$,[5] which means it features no *unstable port-level hidden dynamics*[6] for that port-pair $(i, j)$. This simplified approach, which relies on a single NP, is referred to as *Approach 2b* and is formally stated below.

*Approach 2b:* If for port-pair $(i, j)$ Condition 2 holds, stability of the closed-loop MIMO system $\mathbf{T}(s)$ from (8) and Fig. 2(e), can be determined by applying the NC to the single LAAT loop-gain transfer function $L_{ij}^{\text{LAAT}}(s)$ from (11) [24], [30].

[4]To align with a terminology standardly used in combinatorics, the term "SISO variation" is used in this article to refer to a two-element variation of $N$ elements.

[5]When $i = j$, the port-pair $(i, j)$ is simply referred to as port $i$.

[6]Clarification of the *unstable port-level hidden dynamics* and its differences with respect to the *unstable device-level hidden dynamics*, along with some examples of systems featuring such dynamics is provided in the Appendix.

TABLE I
OVERVIEW OF DIFFERENT STABILITY ASSESSMENT APPROACHES FOR THE MIMO FEEDBACK SYSTEM WITH $N$ INPUTS(OUTPUTS), SUCH AS THE ONE FROM FIG. 2(e), WHICH CORRESPONDS TO AN $N$-PORT INTERLINKING DC–DC CONVERTER

| Impedance based method | Device-level (MIMO) | | Port-level (SISO) | |
|---|---|---|---|---|
| Stability assessed by | Approach 1 | | Approach 2a | Approach 2b |
| Criterion used | determinant GNC | eigenloci GNC | NC | NC |
| Condition 1 required* | yes | yes | yes | yes |
| Condition 2 required | no | no | no | yes |
| NC applied to | $L_m$ | $\forall\lambda_i$ | $\forall L_{ij}^{\text{LAAT}}$ | $L_{ij}^{\text{LAAT}}$ |
| Number of NP | 1 | $N$ | $N^2$ | 1 |

*Condition 1 is required to determine internal stability, but not to determine BIBO stabiltiy.

Along this line, several interesting remarks can be made. First, *Approach 1* and *Approach 2a* always yield the same stability assessment result and thus, for this purpose, can be used indistinguishably [32]. Nevertheless, *Approach 1* may be favorable since it always requires NC to be applied less times, as outlined in Table I and discussed in Section V. Second, Approaches 1, 2a (or 2b) yield *different stability margins*[7] [31], [32]. Finally, it shall be noted that in case Condition 2 is not satisfied for every LAAT SISO variation, i.e., port-pair $(i, j)$, depending on which LAAT SISO variation is chosen, *Approach 2b* may result in inaccurate stability predictions. Thus, without prior knowledge on whether, and for which port-pair, Condition 2 holds, either *Approach 2a* or *Approach 1* must be used to ensure correct stability assessment result.

### C. Relationship With the Standardly Used Port-Level (SISO) Impedance-Based Method

When applying the above discussed approaches for impedance-based stability assessment, given the reasoning from Section II, the loop gain $\mathbf{L}(s)$ of the MIMO feedback system under consideration is the product of the converter's unterminated MIMO admittance matrix and grid's unterminated MIMO impedance matrix, as described by (7). Thereby, the MIMO (*device-level*) impedance-based method from Section II-C relies on directly assessing properties of the MIMO loop gain defined in this way, by using *Approach 1*. On the other hand, the SISO (*port-level*) impedance-based method, which is, by far, the mostly used approach in the literature [2], [4], [6], [10], [11], is founded on a different principle. The subsequent analysis will show that, when applied in its standardly used form, this method involves assessing properties of the corresponding SISO LAAT loop-gain(s) $L_{ii}^{\text{LAAT}}(s)$.

[7]Stability margins, such as phase margin, gain margin or vector (disk) margin, are not univocal parameters in MIMO systems [24], [31], as briefly discussed in Section V. Detailed discussion about merits/demerits of different approaches from the stability margin point-of-view is left for future work, since the most adequate way to define stability margins of a MIMO system is still an open topic also in control systems theory [31].

Recalling (5)–(9), we can write

$$T_{ij}(s) = \left.\frac{\hat{v}_i(s)}{\hat{v}_{gj}(s)}\right|_{\hat{v}_{gk}(s)=0,\hat{i}_{cl}(s)=0} \tag{12}$$

where $i,j,k,l \in \{1,2,\ldots,N\}$ and $k \neq j$. Based on this and (11), each SISO LAAT loop-gain $L_{ij}^{\text{LAAT}}(s)$ can be expressed as a product of an impedance and an admittance

$$L_{ij}^{\text{LAAT}}(s) = Z_{gij}^{t}(s)Y_{ij}^{t}(s) \tag{13}$$

where

$$Y_{ij}^{t}(s) = \left.\frac{\hat{i}_i(s)}{\hat{v}_i(s)}\right|_{\hat{v}_{gk}(s)=0,\hat{i}_{cl}(s)=0} \tag{14}$$

$i,j,k,l \in \{1,2,\ldots,N\}$ and $k \neq j$, is termed converter's *terminated* admittance for port-pair $(i,j)$ and

$$Z_{gij}^{t}(s) = \left.\frac{\hat{v}_{gj}(s) - \hat{v}_i(s)}{\hat{i}_i(s)}\right|_{\hat{v}_{gk}(s)=0,\hat{i}_{cl}(s)=0} \tag{15}$$

is termed grid's *terminated* impedance for port-pair $(i,j)$. Thus, relying on *Approach 2a* or *Approach 2b*, the SISO impedance-based method involves evaluating LAAT minor-loop gain(s) $L_{ij}^{\text{LAAT}}(s) = Z_{gij}^{t}(s)Y_{ij}^{t}(s)$, given by (11). Thereby, depending on whether *Approach 2a* or *Approach 2b* is used, stability check is performed for, respectively, every possible or a single port-pair.

Still, in the existing literature on the SISO impedance based stability assessment [2], [4], [6], [10], [11], only *Approach 2b* is typically used, applied to one of the ports, i.e., a single $L_{ii}^{\text{LAAT}}(s) = Z_{gii}^{t}(s)Y_{ii}^{t}(s)$ is assessed. However, this is not generally applicable, since it does not always guarantee accurate BIBO stability prediction (as elaborated in the previous subsection), due to possible, *unstable port-level hidden dynamics*.[8]

As a partial generalization, evaluation of all $L_{ii}^{\text{LAAT}}(s)$ is sometimes performed (which corresponds to applying the SISO method at every port) [5], [6], [8], [16]. For example, in [5], stability of the voltage source converter in nonmeshed HVDC system featuring *unstable port-level hidden dynamics* at the dc port could not have been accurately predicted by applying the SISO impedance based method to that port. Rather, the SISO method had to be applied to the ac port.

Still, even the evaluation of all $L_{ii}^{\text{LAAT}}(s)$ may not always be sufficient. Namely, even though for $i \neq j$ $Z_{gij}^{t}(s)$ and $Y_{ij}^{t}(s)$ provide little physical insight, also all $L_{ij}^{\text{LAAT}}(s) = Z_{gij}^{t}(s)Y_{ij}^{t}(s)$ must be evaluated (*Approach 2a* must be used) to account for possible *unstable port-level hidden dynamics*, which, in a general case, may arise for any port-pair. Such scenarios can be considered likely to appear in modern power electronics systems with meshed structures.

For meshed systems, even in absence of any *unstable port-level hidden dynamics*, though mathematically-wise correct, the SISO impedance-based stability assessment has no intuitive physical interpretation. This is because for such systems, where both $\mathbf{Y}(s)$ and $\mathbf{Z_g}(s)$ are nondiagonal, as one can derive from (14) and (15), $Z_{gij}^{t}(s)$ and $Y_{ij}^{t}(s)$ depend on all elements of both $\mathbf{Y}(s)$ and $\mathbf{Z_g}(s)$, i.e., they are all coupled. This is probably the reason why, to the best of authors' knowledge, the SISO impedance-based stability assessment has so far been used only in nonmeshed systems. Thus, to provide a clear understanding and the correlation of the above presented with the way SISO impedance-based method is standardly used [2], [6], [10], [11], a nonmeshed variant of the system from Fig. 2(a) is considered and the application of the SISO method to one of the ports is illustrated as follows.

When applied to port $i$ ($i = 1$ or $i = 2$), the SISO impedance-based method relies on the converter's *terminated* admittance $Y_{ii}^{t}(s)$ and the grid's *terminated* impedance $Z_{gii}^{t}(s)$, seen at that port. For a nonmeshed system with a diagonal $\mathbf{Z_g}(s)$ [given by (4)] and a nondiagonal $\mathbf{Y}(s)$ [given by (1)], which is hereafter considered, it can be derived from (15) that $Z_{g11}^{t}(s) = Z_{g11}$ and $Z_{g22}^{t}(s) = Z_{g22}$. Similarly, (14) yields

$$Y_{11}^{t}(s) = Y_{11}(s) - \frac{Y_{12}(s)Y_{21}(s)Z_{g22}(s)}{1 + Y_{22}(s)Z_{g22}(s)} \tag{16}$$

and

$$Y_{22}^{t}(s) = Y_{22}(s) - \frac{Y_{12}(s)Y_{21}(s)Z_{g11}(s)}{1 + Y_{11}(s)Z_{g11}(s)}. \tag{17}$$

Subsequently, depending on whether the SISO impedance-based method is applied to port 1 or to port 2, the circuit from Fig. 2(a) can be simplified to the one in Fig. 2(c) or (d). According to Fig. 2(c), the following holds:

$$\hat{v}_1(s)|_{\hat{i}_{c1}^{t}(s)=0} = \frac{\hat{v}_{g1}(s)}{1 + Y_{11}^{t}(s)Z_{g11}^{t}(s)} \tag{18}$$

$$\hat{i}_1(s)|_{\hat{v}_{g1}(s)=0} = \frac{\hat{i}_{c1}^{t}(s)}{1 + Y_{11}^{t}(s)Z_{g11}^{t}(s)} \tag{19}$$

where according to Fig. 2(a), $\hat{i}_{c1}^{t}(s)$ is for the considered nonmeshed system given by

$$\hat{i}_{c1}^{t}(s) = \hat{i}_1(s)|_{\hat{v}_1(s)=0} = \hat{i}_{c1}(s) + \frac{Y_{12}(s)\hat{v}_{g2}(s)}{1 + Z_{g22}(s)Y_{22}(s)}. \tag{20}$$

Similarly, according to Fig. 2(d), the following holds:

$$\hat{v}_2(s)|_{\hat{i}_{c2}^{t}(s)=0} = \frac{\hat{v}_{g2}(s)}{1 + Y_{22}^{t}(s)Z_{g22}(s)} \tag{21}$$

$$\hat{i}_2(s)|_{\hat{v}_{g2}(s)=0} = \frac{\hat{i}_{c2}^{t}(s)}{1 + Y_{22}^{t}(s)Z_{g22}(s)} \tag{22}$$

where, according to Fig. 2(a), $\hat{i}_{c2}^{t}(s)$ is for the considered nonmeshed system given by

$$\hat{i}_{c2}^{t}(s) = \hat{i}_2(s)|_{\hat{v}_2(s)=0} = \hat{i}_{c2}(s) + \frac{Y_{21}(s)\hat{v}_{g1}(s)}{1 + Z_{g11}(s)Y_{11}(s)}. \tag{23}$$

The expressions such as (18)–(19) and (21)–(22), in fact, motivated the development and wide application of the SISO impedance-based method at a port of interest [2], [6], [10], [11]. For this, similarly as in Section II-C, the grid and the converter are assumed to be standalone stable. Then, according to (18) and

[8]For power electronic systems, some examples of limited *port-level* observability and/or controllablilty, as well as the absence of it (which corresponds to *port-level hidden dynamics*), are reported in [5], [8], [15], [16], [17].

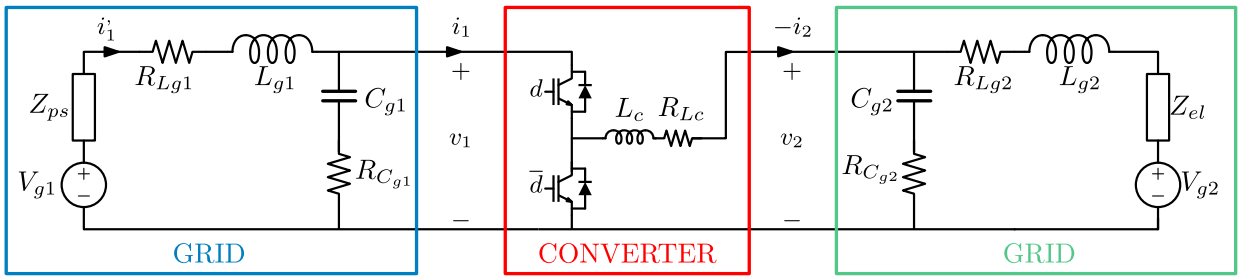


Fig. 4. Circuit representing a simple example of a DC system from Fig. 1, which is used to illustrate the presented methodology analytically, in HIL simulations and experimentally. The system consists of a nonmeshed grid and the current-controlled buck converter, which is used as an example of a two-port interlinking converter. The circuit parameters are provided in Table II.

(19) [or (21) and (22)] stability of the interconnected system can be determined by checking the stability of the SISO closed-loop system from Fig. 2(f) [or Fig. 2(g)], where

$$L_{11}^{LAAT}(s) = Z_{g11}^{t}(s)Y_{11}^{t}(s) = Z_{g11}(s)Y_{11}^{t}(s) \tag{24}$$

$$L_{22}^{LAAT}(s) = Z_{g22}^{t}(s)Y_{22}^{t}(s) = Z_{g22}(s)Y_{22}^{t}(s) \tag{25}$$

are the corresponding, so-called minor, loop-gains for the SISO impedance-based stability assessment at port 1 and at port 2, respectively. Nevertheless, given the theory from Section III-B, it shall be underlined once again that stability assessment of solely $L_{11}^{\mathrm{LAAT}}(s)$ or $L_{22}^{\mathrm{LAAT}}(s)$ is sufficient to determine stability of an interconnected nonmeshed two-port system only if, for the considered port, Condition 2 holds. Otherwise, along with the more intuitive handling of multiport and meshed systems, etc. the use of the MIMO impedance-based method is recommended, as discussed in Section V.

## IV. Application Example and Validation

### A. Considered Test-Case

To illustrate the use of the previously discussed stability assessment approaches, a simple nonmeshed system resembling the one from Fig. 1(b) is considered, which is shown in Fig. 4 and features parameters from Table II, which were adopted as an example. Note that the applicability of the methodology presented in this article is not limited to the specific grid/converter parameter choice; rather, the methodology is of general use and remains valid for any parameter values. The system under study consists of a digital pulsewidth modulated current-controlled two-level buck converter and a grid. The grid's dc bus voltages are formed by a constant voltage source and a constant voltage load. The grid's impedances are realized by passive *LC* elements.[9] The grid's impedances thus feature resonances which threaten to endanger system stability.

First, it was of interest to analytically predict stability properties of such a system, by applying the SISO impedance-based method (*Approach 2b*)[10] for the port-pairs (1,1) and (2,2), i.e., ports 1 and 2, as well as the MIMO impedance-based method (*Approach 1*). For this, the elements of the grid impedance matrix, $Z_{g11}(s)$, $Z_{g22}(s)$, and the converter's admittance matrix $Y_{11}(s)$, $Y_{22}(s)$, $Y_{21}(s)$, $Y_{12}(s)$ are at first calculated, based on Fig. 4, Table II and the small-signal $s$-domain model of the converter and its closed-loop control system.[11] The resulting frequency responses of the converter's admittances are obtained for two different values of the current reference $I_{\mathrm{ref}} = 5$ A and $I_{\mathrm{ref}} = 20$ A. Due to space limitations, only the results for $I_{\mathrm{ref}} = 20$ A are shown (with full-lines) in Fig. 5. The resulting frequency responses of the grid's impedances are shown (with full lines) in Fig. 6. Then, the minor loop-gains $L_{11}^{\mathrm{LAAT}}$, $L_{22}^{\mathrm{LAAT}}$, $\mathbf{L}$ are calculated based on (7), (24), and (25), and the NC is

TABLE II
Parameters of the Tested Converter and the Grid

| Buck converter's parameters | label | value | unit |
|---|---|---|---|
| Input voltage | $V_{g1}$ | 48 | V |
| Output voltage | $V_{g2}$ | 36 | V |
| Filter inductance | $L_c$ | 1.5 | mH |
| Inductor's series resistance | $R_{\mathrm{L_c}}$ | 0.25 | Ω |
| Switching frequency | $f_{pwn}$ | 5 | kHz |
| Control update frequency | $f_c$ | 10 | kHz |
| Crossover frequency | $f_{cr}$ | 1 | kHz |
| **Grid's resonance 1 parameters** | **label** | **value** | **unit** |
| Inductance | $L_{g1}$ | 72 | μH |
| Inductor's series resistance | $R_{L_{g1}}$ | 15 | mΩ |
| Capacitance | $C_{g1}$ | 235 | μF |
| Capacitor's series resistance | $R_{C_{g1}}$ | 75 | mΩ |
| **Grid's resonance 2 parameters** | **label** | **value** | **unit** |
| Inductance | $L_{g2}$ | 360 | μH |
| Inductor's series resistance | $R_{L_{g2}}$ | 20 | mΩ |
| Capacitance | $C_{g2}$ | 170 | μF |
| Capacitor's series resistance | $R_{C_{g2}}$ | 5 | mΩ |

[9]The impedances $Z_{ps} = R_{ps}||(sL_{ps})$ and $Z_{el}(s) = R_{el}||(1/(sC_{el}))||(sL_{el})$, which are also contributing to grid impedances, are included in Fig. 4 to match the experimentally tested circuit, discussed in Section IV-C. More precisely, these impedances account for the non-ideal dynamics of the electronic source and load used for experimental validation.

[10]The considered system does not feature *unstable port-level hidden dynamics* for port-pairs (1,1) and (2,2) and thus it was sufficient to apply *Approach 2b* to either of these port-pairs (ports).

[11]In the considered case, which includes a current-controlled buck converter, the expressions for $Y_{11}(s)$, $Y_{22}(s)$, $Y_{21}(s)$, $Y_{12}(s)$ can be found in [26].

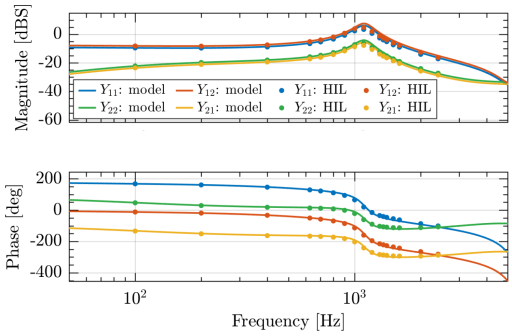


Fig. 5. Frequency responses of the converter's unterminated MIMO impedance matrix elements, corresponding to the system from Fig. 4 with $I_{\text{ref}} = 20$ A. Comparison between the results obtained using analytical model (full lines) and HIL simulations (dots).

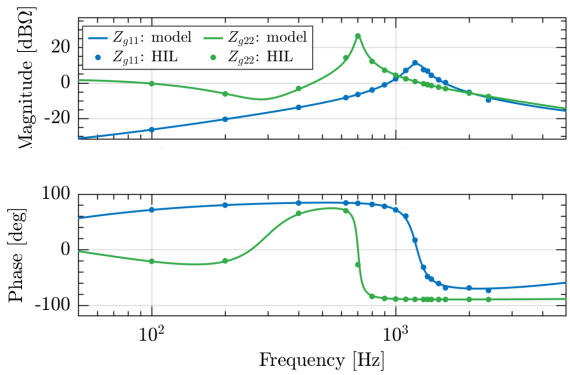


Fig. 6. Frequency responses of the grid's unterminated MIMO impedance matrix elements, corresponding to the system from Fig. 4. Comparison between the results obtained using analytical model (full lines) and HIL simulations (dots).

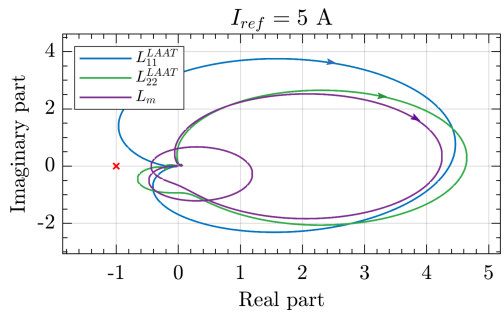


Fig. 7. NPs used for the stability assessment of the system from Fig. 4 with the parameters from Table II and $I_{\text{ref}} = 5$ A. The blue, green and purple plots, denoted by $L_{11}^{\text{LAAT}}$, $L_{22}^{\text{LAAT}}$, and $L_m$, correspond to, respectively. Approach 2b applied to port 1, Approach 2b applied to port 2, and Approach 1. Stable response is predicted by all three approaches.

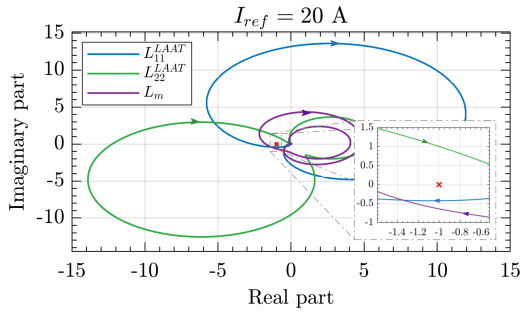


Fig. 8. NPs used for the stability assessment of the system from Fig. 4 with the parameters from Table II and $I_{\text{ref}} = 20$ A. The blue, green, and purple plots, denoted by $L_{11}^{\text{LAAT}}$, $L_{22}^{\text{LAAT}}$, and $L_m$, correspond to, respectively. Approach 2b applied to port 1, Approach 2b applied to port 2, and Approach 1. Instability is predicted by all three approaches.

applied to $L_{11}^{\text{LAAT}}$ and $L_{22}^{\text{LAAT}}$, while the determinant-based GNC is applied to $\mathbf{L}$. The corresponding NPs of $L_{11}^{\text{LAAT}}$, $L_{22}^{\text{LAAT}}$ and $L_m$ [from (10)] are shown in Figs. 7 and 8, for $I_{\text{ref}} = 5$ A and $I_{\text{ref}} = 20$ A. Given that in neither case the minor loop gains contain RHP poles, stability of the interconnected system can be judged by checking whether the corresponding Nyquist curve encircles the critical $(-1,0)$ point. As seen, for $I_{\text{ref}} = 5$ A, none of the three plotted curves, $L_{11}^{\text{LAAT}}$, $L_{22}^{\text{LAAT}}$, and $L_m$ feature such encirclement. Thus, all three considered approaches predict a stable response. On the other hand, when $I_{\text{ref}} = 20$ A, instability is predicted by all three approaches, since the corresponding Nyquist curves all encircle $(-1,0)$. Note that, since the considered system does not feature *unstable port-level hidden dynamics* for neither port 1 nor port 2, all three considered approaches, *Approach 1*, *Approach 2b* at port 1, and *Approach 2b* at port 2, in each considered scenario (Figs. 7 and 8), yielded the same stability prediction result. Thus, for solely determining whether the system will be stable or unstable, they can be used indistinguishably in the considered simple example. However, the three methods yield different stability margins, as seen from Fig. 7. Furthermore, as discussed in Section V, *Approach 1* may be favorable in systems with meshed structures, multiport converters or *unstable port-level hidden dynamics*, as well as for development of the robust termination-independent stabilization methods and stability assessment based on measurements.

### B. HIL Validation

To verify the analytical stability predictions from previous subsection, real-time control-HIL (C-HIL) simulations of the system from Fig. 4 are performed. For this, Typhoon HIL 402 is used to emulate the converter and the grid, with the circuit solver time step set to 0.5 $\mu$s. The inductor current is acquired from the HIL's analog output. Analog-to-digital-conversion (ADC), the current control and DPWM are realized in the digital signal processor (DSP) within Imperix B-Board PRO control platform. The same parameters (provided in Table II) are used as for the results in Figs. 5–8.

To validate that the realized system faithfully models dynamics of the one used for analytical predictions, frequency response measurements are performed to obtain $Z_{g11}(j\omega)$, $Z_{g22}(j\omega)$ and $Y_{11}(j\omega)$, $Y_{12}(j\omega)$, $Y_{21}(j\omega)$, $Y_{22}(j\omega)$ for $I_{\text{ref}} = 5$ A and $I_{\text{ref}} = 20$ A. For this, the series perturbation injection circuits were emulated in HIL, and the HIL's dedicated SCADA widget was used to obtain the frequency responses of interest, which are plotted (with dots) in Figs. 5 and 6. As seen, the results obtained from HIL measurements are excellently matching those obtained from analytical models. Thus, the analytical stability predictions are expected to match the stability properties of the system realized using HIL.

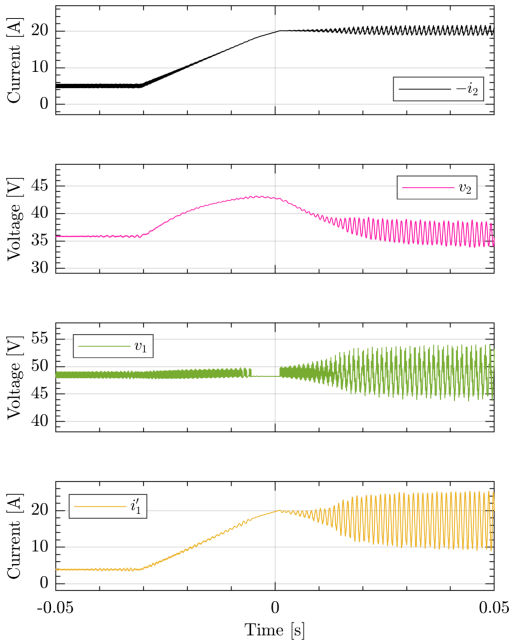


Fig. 9. Response of the circuit from Fig. 4 to the reference ramp change from $I_{\text{ref}} = 5$ A to $I_{\text{ref}} = 20$ A, obtained using HIL simulations. As predicted in Fig. 8, instability arises for $I_{\text{ref}} = 20$ A.

To verify this, the converter's input and output voltage and current waveforms in response to the ramp change of the inductor current reference from $I_{\text{ref}} = 5$ A to $I_{\text{ref}} = 20$ A are shown in Fig. 9. As predicted in Figs. 7 and 8, for $I_{\text{ref}} = 5$ A a stable operation is achieved, while an instability arises when the reference reaches $I_{\text{ref}} = 20$ A.

### C. Experimental Validation

To further validate analytical predictions of different stability assessment approaches discussed in previous sections, the laboratory prototype of the system from Fig. 4 is built, featuring, same as previously, parameters from Table II. The picture of the test setup is shown in Fig. 10. The converter is realized using PEB8024 SiC half bridge modules from Imperix, and passive *LC* elements are used for the converter's inductive filter and the grid impedances. The dc voltages at the converter's input and output ports are provided by the dc power supply Chroma 62050P-100-100 and the electronic load EA-EL 9750-120 B. The inductor current is sensed by the built-in LEM-based current sensor from Imperix. The realization of the digital current control is the same as the one used for HIL simulations, compiled to another control platform (B-Box RCP from Imperix), which is compatible with the hardware used for the power stage and features the same DSP as the one used for HIL validations. Time domain stability test is performed, in the same way as before. The ramp change of the inductor current reference from $I_{\text{ref}} = 5$ A to $I_{\text{ref}} = 20$ A is imposed and the converter's input and output voltage and current waveforms are captured by an oscilloscope. The captured responses are shown in Fig. 11. As predicted in Figs. 7 and 8, and previously verified using HIL, the experimentally tested system achieves stable operation for $I_{\text{ref}} = 5$ A, while, due to interactions between the converter and the grid, the system gets destabilized for $I_{\text{ref}} = 20$ A.

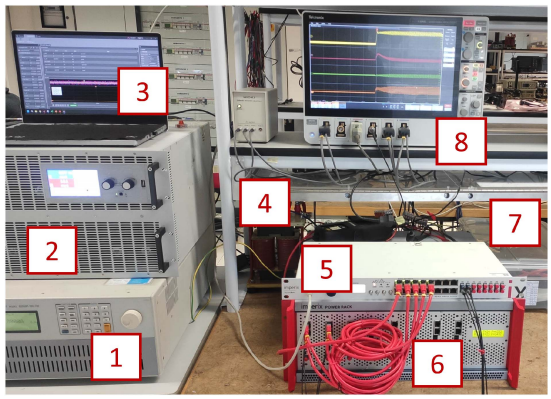


Fig. 10. Test-setup used for experimental validation: 1) input DC power supply Chroma 62050P-100-100; 2) electronic load EA-EL 9750-120; 3) laptop; 4) filter inductor; 5) Boom Box controller; 6) SiC half-bridge modules; 7) passive elements used to form grid resonances; 8) Tektronix MS056 oscilloscope.

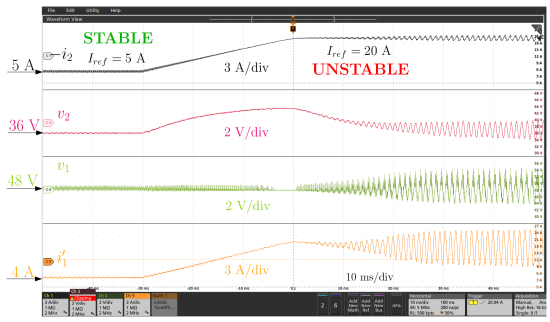


Fig. 11. Experimentally measured response of the circuit from Fig. 4 (realized using the prototype from Fig. 10) to the current reference ramp change from $I_{\text{ref}} = 5$ A to $I_{\text{ref}} = 20$ A. As predicted in Fig. 8, instability arises for $I_{\text{ref}} = 20$ A.

## V. Merits and Limitations of SISO and MIMO Impedance-Based Methods

Given all of the above presented, it is of interest to comment on the strengths and weaknesses of the MIMO (*device-level*), and the SISO (*port-level*) impedance-based method for the stability assessment of dc–dc interlinking converters in grid-connecting scenarios. The methods are compared based on several different indicators: 1) computational complexity required to account for the *unstable port-level hidden dynamics*; 2) suitability for multiport interlinking converters; 3) applicability in meshed grids; 4) potentials from the stability margins point of view; 5) appropriateness for termination-independent stability-oriented controller design; 6) applicability for the stability assessment based on measurements.

When it is of interest to determine stability without prior knowledge on whether (and for which port-pair) there could be *unstable port-level hidden dynamics*, either the MIMO method (which corresponds to *Approach 1*) or the SISO method applied to every possible port-pair (which corresponds to *Approach 2a*)

can be used. Thereby, the MIMO method may be more convenient to use than the SISO one, as it is able to account for *unstable port-level hidden dynamics* with a single NP (by using determinant-based GNC). This advantage, as illustrated in Table I, gets further emphasized as the number of ports (inputs/outputs) increases.

When it is known in advance that for a certain port-pair, the *unstable port-level hidden dynamics* do not appear, as in the example from Section IV, both the MIMO method (*Approach 1*) and the SISO method applied to that single port-pair (*Approach 2b*) can be used to accurately assess stability. Consequently, if the determinant-based GNC is used for the former, both methods rely on a single NP. Still, the MIMO method may be favorable for analytical stability predictions due to its modularity and scalability. For example, its extension to systems with higher number of ports, such as multiport converters, is straightforward. On the contrary, the complexity of expressions for the SISO method, more specifically, for terminated immittances (such as (16) and (17)) significantly increases as the number of ports increases [33].

As for the stability assessment of an interlinking converter in meshed grids, the MIMO impedance-based method inherently and intuitively handles this scenario, since with this approach, the subsystems' immittances to be evaluated are defined in the *all-port* MIMO *unterminated* sense. On the contrary, though theoretically wise possible to use for analytical stability assessment, the SISO impedance based-approach loses intuitiveness and provides little physical insight in meshed systems. This is because the interconnected system gets fully coupled and, consequently, the subsystems' *terminated* immittances become dependent on all of both subsystems' unterminated immittances.

Regarding the stability margins, provided that no *port-level hidden dynamics* appear, both SISO and MIMO methods may be useful, depending on the information of interest. The SISO method allows to determine stability margins of a single output when exposed to a perturbation at a single input, whereas the MIMO method allows to determine stability margins of all outputs when exposed to simultaneous perturbations at all inputs [24], [31]. Compared to the MIMO method using determinant-based GNC, the MIMO method using eigenloci-based GNC, as well as the SISO method, may provide more insight on where the risk for destabilization comes from [32]. Nevertheless, with the determinant-based MIMO method, definition of a single stability margin is straightforward [31]. Though interpretation of all these stability margins is different, it is important to emphasize that they all reflect properties of the same converter's control system. Thus, it may be difficult to control them independently in practice. Research along this line is left for future studies.

Next, it is of interest to comment on the applicability and suitability of the SISO and MIMO impedance-based methods for the robust stability-oriented controller design. The goal of such design strategies is to ensure stability even when termination varies, which, as explained below, may be difficult using converter's *terminated* immittances. As one example of such strategies, admittance passivity-oriented controller design [12], [14], [26] is considered below. Stemming from the SISO impedance-based method, the conventional admittance passivity-oriented design concepts strive for passivizing the converter's (*terminated*) SISO admittance at a connection port. However, this requires assumptions about termination at all other converter's ports, limiting thereby the applicability of such a concept for preventing port-coupling induced instability [26]. On the contrary, by aiming to passivize the converter's unterminated MIMO admittance matrix, stability can be ensured for an arbitrary (even-meshed) passive termination [26]. This concept, which was for the first time proposed by Cvetanovic et al. [26], naturally comes to one's mind if, for evaluating stability, instead of the standardly used SISO, the MIMO impedance-based method is considered. More details along this line can be found in [26].

Finally, when the stability assessment of an $N$-port interlinking converter is to be performed based on measurements, rather than analytical models, the MIMO method may again be advantageous. Namely, for such stability assessment, frequency responses of the immittances that appear in the minor-loop gain, which is to be evaluated, must be first measured. To avoid potential instability that may arise when the considered converter is, even at a single port, connected to the grid of interest, such measurements (and subsequent stability assessments) must be first performed under the termination for which the converter's control system is known to be stable, which typically corresponds to zero grid impedances (ideal termination). Frequency responses of the *unterminated* immittances that can be obtained in this way [19] are sufficient to apply the MIMO method. However, as elaborated in Section III, application of the SISO method relies on the specific *terminated* immittances. Measurement of these immittances at the port of interest requires terminating the converter at all other ports by the grid impedances that correspond to the scenario for which stability is to be assessed. Thus, prior to measuring the terminated immittances required for the SISO stability assessment at the port of interest, the SISO stability assessments at all other ports must be performed, using the corresponding *unterminated* immittances. Consequently, for the stability assessment based on measurements, even in absence of any *unstable port-level hidden dynamics*, the SISO method would have to be applied more than once ($N$ times). Thus, though in this case, the number of the required frequency response measurements, i.e., independent perturbation injections, remains the same for the SISO and the MIMO method, the MIMO method may be preferable as it allows NC to be applied only once (if the determinant-based GNC is used). In addition, in case the stability assessment is to be repeated once termination changes, the MIMO method would require less additional measurements (and assessments). Furthermore, if the system is meshed, using the SISO method for the stability assessment based on measurements is feasible only in case the converter remains stable when connected to the grid of interest. This is because, contrary to nonmeshed system, measurement of terminated immittances in meshed system requires the converter to be operated under the conditions for which stability assessment is to be performed, since, as explained in Section III-C, terminated immittances are in this case fully coupled.

## VI. Conclusion

By relying on the formal control systems theory principles, this article provides the correlation and the comparison between the standardly used *port-level* (terminated) SISO, and the recently acknowledged *device-level* (unterminated) MIMO impedance-based method for the stability assessment of dc–dc interlinking converters. The capability of these methods to account for *(unstable) port-level hidden dynamics* is for the first time discussed and the MIMO method is revealed to be preferable for this purpose. The suitability of the SISO and the MIMO methods for stability assessment in systems with meshed structures and/or multiport converters, as well as for defining various stability margins is also addressed, again showing that the MIMO method is advantageous. Moreover, the unterminated (black-box) representation-related assets of the MIMO method are highlighted, which are relevant when the stability is to be assessed based on measurements, as well as when robust stability-oriented termination-independent control strategies are to be designed. The presented methodology is validated in HIL simulations and experimentally, using the laboratory prototype of a current-controlled buck converter. Future studies will focus on extending the presented methodology to ac–dc systems.

## Appendix A

Consider an arbitrary continuous LTI system $\Sigma_G$ whose state-space representation is given by

$$\begin{aligned}\frac{d\mathbf{x}(t)}{dt} &= \mathbf{A_G}\cdot\mathbf{x}(t)+\mathbf{B_G}\cdot\mathbf{u}(t)\\ \mathbf{y}(t) &= \mathbf{C_G}\cdot\mathbf{x}(t)+\mathbf{D_G}\cdot\mathbf{u}(t)\end{aligned} \tag{26}$$

where $\mathbf{x}(t)\in\mathbb{R}^{N_x}$, $\mathbf{u}(t)\in\mathbb{R}^{N_u}$, and $\mathbf{y}(t)\in\mathbb{R}^{N_y}$ denote, respectively, system states, inputs, and outputs, the number of each being $N_x$, $N_u$, and $N_y$, and $\mathbf{A_G}$, $\mathbf{B_G}$, $\mathbf{C_G}$, and $\mathbf{D_G}$ are appropriately dimensioned real constant matrices [30]. The corresponding transfer function (matrix) from $\mathbf{u}$ to $\mathbf{y}$ is given by [30]

$$\mathbf{G}(s)=\mathbf{C_G}\cdot(s\mathbf{I}-\mathbf{A_G})^{-1}\cdot\mathbf{B_G}+\mathbf{D_G}. \tag{27}$$

The system $\Sigma_G$ is internally stable if all the eigenvalues (modes) $\lambda_{A_G}=\{\lambda_1,\lambda_2,\ldots\lambda_{N_x}\}$ of $\mathbf{A_G}$ are in the open left-half plane, while it is externally (input–output or BIBO) stable if all the poles $p_G=\{p_1,p_2,\ldots\}$ of $\mathbf{G}$ are in the open left-half plane [30]. The possible difference between the two stabilities (internal and external) stems from the fact that not all the eigenvalues of $\mathbf{A_G}$ are necessarily the poles [34] of $\mathbf{G}(s)$, due to possible pole-zero cancellations [30]. This occurs in case the system $\Sigma_G$ is not controllable or observable, which are the properties defined as follows.[12] The system $\Sigma_G$ is called controllable if the below stated Condition A.1 holds.

*Condition A.1:* The matrix

$$\mathbf{P}=[\mathbf{A_G}-\lambda\mathbf{I},\mathbf{B_G}] \tag{28}$$

for all $\lambda=\{\lambda_i\in\lambda_{A_G}\}$ has full row rank [30].

Similarly, the system $\Sigma_G$ is called observable if the below stated Condition A.2 holds.

*Condition A.2:* The matrix

$$\mathbf{Q}=[\mathbf{A_G}-\lambda\mathbf{I},\mathbf{C_G}]^T \tag{29}$$

for all $\lambda=\{\lambda_i\in\lambda_{A_G}\}$ has full column rank [30].

If the system $\Sigma_G$ is not observable or controllable (Condition A.1 or Condition A.2 does not hold), it is, in this article, said to feature *hidden dynamics*. In this case its internal stability may be different from BIBO stability, i.e., instability may arise that can not be predicted by evaluating poles of $\mathbf{G}(s)$. Still, even when the system features *hidden dynamics*, internal stability can be accurately predicted from $\mathbf{G}(s)$ [30] in case the system $\Sigma_G$ is stabilizable and detectable, which are the properties defined as follows. The system $\Sigma_G$ is called stabilizable if the below stated Condition A.3 holds.

*Condition A.3:* The matrix (28) for all $\lambda=\{\lambda_i\in\lambda_{A_G}\mid Re\{\lambda_i\geq 0\}\}$, has full row rank.

Similarly, the system $\Sigma_G$ is called detectable if the below stated Condition A.4 holds.

*Condition A.4:* The matrix (29), for all $\lambda=\{\lambda_i\in\lambda_{A_G}\mid Re\{\lambda_i\geq 0\}\}$, has full column rank.

Based on the definitions above, it is now of interest to distinguish between the *unstable device-level hidden dynamics* and the *unstable port-level hidden dynamics*, the properties being mentioned in Section III. For this, the LTI MIMO system $\Sigma_T$ (such as one from Section III) is considered hereafter, which is characterized by the state-space representation from (26), where $\mathbf{A_G}=\mathbf{A_T}$, $\mathbf{B_G}=\mathbf{B_T}$, $\mathbf{C_G}=\mathbf{C_T}$, $\mathbf{D_G}=\mathbf{D_T}$ and $N_x=N_{x_T}$, $N_u=N_{u_T}$, $N_y=N_{y_T}$. The corresponding transfer function matrix $\mathbf{T}(s)$ can be obtained from (27). The elements of $\mathbf{T}(s)$ are $T_{ij}(s)$, where $i\in\{1,2,\ldots N_{u_T}\}$ and $j\in\{1,2,\ldots N_{y_T}\}$. Each $T_{ij}(s)$ is the transfer function of the SISO system $\Sigma_{T_{ij}}$, which is characterized by the state space representation from (26), where[13] $\mathbf{A_G}=\mathbf{A_{T_{ij}}}$, $\mathbf{B_G}=\mathbf{B_{T_{ij}}}$, $\mathbf{C_G}=\mathbf{C_{T_{ij}}}$, $\mathbf{D_G}=D_{T_{ij}}$ and $N_x=N_{x_{T_{ij}}}$, $N_u=1$, $N_y=1$.

If the considered MIMO system $\Sigma_T$ satisfies Condition A.3 and Condition A.4, this system is said not to feature *unstable device-level hidden dynamics*. As such, it is detectable and stabilizable in a MIMO sense, i.e., its internal stability can be accurately predicted by evaluating the poles of its transfer function matrix $\mathbf{T}(s)$. If the SISO system $\Sigma_{T_{ij}}$ satisfies Condition A.3 and Condition A.4, the considered MIMO system $\Sigma_T$ is said not to feature *unstable port-level hidden dynamics* for a SISO variation, i.e., port-pair $(i,j)$. In this case, the considered MIMO system $\Sigma_T$ is detectable and stabilizable for a single SISO variation $(i,j)$ (in a SISO sense). Consequently, the BIBO stability of the MIMO system $\Sigma_T$ is equivalent to the BIBO stability of the SISO system $\Sigma_{T_{ij}}$, which can be accurately predicted by evaluating the poles of the transfer function $T_{ij}$. Nevertheless, without prior knowledge on whether the considered MIMO system $\Sigma_T$ features any *unstable port-level hidden dynamics*, the poles of all $T_{ij}$ must be evaluated to accurately determine (BIBO) stability of the MIMO system $\Sigma_T$. As explained in

[12] All the subsequent definitions apply regardless of whether the system $\Sigma_G$ is SISO ($N_u=N_y=1$) or MIMO ($N_u>1, N_y>1$) system.

[13] $\mathbf{A_{T_{ij}}}$, $\mathbf{B_{T_{ij}}}$, $\mathbf{C_{T_{ij}}}$, and $D_{T_{ij}}$ can be determined from $\mathbf{A_T}$, $\mathbf{B_T}$, $\mathbf{C_T}$, and $\mathbf{D_T}$.

Section III-B, this is very important if it is of interest to use the SISO-based tools to determine (BIBO) stability of the MIMO system [30], which is often called LAAT approach.

To illustrate the above outlined properties, some examples are provided as follows.

*Example 1:* Consider an LTI MIMO system $\Sigma_T$, whose matrices describing the state-space representation are

$$\mathbf{A_T} = \begin{bmatrix} 1 & -4 \\ -1 & -2 \end{bmatrix}, \mathbf{B_T} = \begin{bmatrix} 1 & -1 \\ 1 & -1 \end{bmatrix}$$
$$\mathbf{C_T} = \begin{bmatrix} 1 & 1 \\ 3 & 2 \end{bmatrix}, \mathbf{D_T} = \begin{bmatrix} 0 & 0 \\ 0 & 0 \end{bmatrix}.$$

Such system features two eigenvalues $\lambda_1 = -3$ and $\lambda_2 = 2$. According to (27), the corresponding input–output transfer function matrix is given by

$$\mathbf{T}(s) = \begin{bmatrix} \frac{2}{s+3} & -\frac{2}{s+3} \\ \frac{5}{s+3} & -\frac{5}{s+3} \end{bmatrix}.$$

It features one pole $p_1 = -3$. By checking the above outlined conditions, it can be shown that the system $\Sigma_T$ is observable, and thus detectable, but neither controllable nor stabilizable. As such, it features *unstable device-level hidden dynamics*, and hence, though BIBO stable ($Re\{p_1\} < 0$) it is internally unstable ($\lambda_2 > 0$).

*Example 2:* Consider an LTI MIMO system $\Sigma_T$, whose matrices describing the state-space representation are

$$\mathbf{A_T} = \begin{bmatrix} 1 & 0 \\ 0 & -3 \end{bmatrix}, \mathbf{B_T} = \begin{bmatrix} 1 & 0 \\ 0 & 1 \end{bmatrix}$$
$$\mathbf{C_T} = \begin{bmatrix} 1 & 0 \\ 0 & 1 \end{bmatrix}, \mathbf{D_T} = \begin{bmatrix} 0 & 0 \\ 0 & 0 \end{bmatrix}.$$

Such system features two eigenvalues $\lambda_1 = -3$ and $\lambda_2 = 1$. According to (27), the corresponding input–output transfer function matrix is given by

$$\mathbf{T}(s) = \begin{bmatrix} \frac{1}{s-1} & 0 \\ 0 & \frac{1}{s+3} \end{bmatrix} = \begin{bmatrix} T_{11}(s) & 0 \\ 0 & T_{22}(s) \end{bmatrix}.$$

It features two poles $p_1 = -3$ and $p_2 = 1$. By checking the above outlined conditions, it can be shown that the system $\Sigma_T$ is both controllable (and thus stabilizable) and observable (and thus detectable). As such, it does not feature *device-level hidden dynamics*, and its internal stability is equivalent to BIBO stability, which can be determined by evaluating poles of $\mathbf{T}(s)$. Therefore, since $Re\{p_2\} > 0$, the system is unstable.

Along this line, it is of interest to check whether the stability of the considered MIMO system $\Sigma_T$ can also be accurately predicted by evaluating poles of a single element of $\mathbf{T}(s)$. For this, as previously explained, the above outlined conditions should be checked for the SISO subsystems $\Sigma_{T_{ij}}$. Given the state-space representation of the considered MIMO system $\Sigma_T$, the state-space representation of each SISO subsystems $\Sigma_{T_{ij}}$ can be determined. Since in the considered example $\mathbf{T}(s)$ is diagonal matrix, only two "nonzero" SISO subsystems exist: $\Sigma_{T_{11}}$ and $\Sigma_{T_{22}}$. Accordingly, the state-space representation of $\Sigma_{T_{11}}$ is given by

$$\mathbf{A_{T_{11}}} = \begin{bmatrix} 1 & 0 \\ 0 & -3 \end{bmatrix}, \mathbf{B_{T_{11}}} = \begin{bmatrix} 1 \\ 0 \end{bmatrix}$$
$$\mathbf{C_{T_{11}}} = [1 \quad 0], \mathbf{D_{T_{11}}} = [0].$$

Similarly, the state-space representation of $\Sigma_{T_{22}}$ is given by

$$\mathbf{A_{T_{22}}} = \begin{bmatrix} 1 & 0 \\ 0 & -3 \end{bmatrix}, \mathbf{B_{T_{22}}} = \begin{bmatrix} 0 \\ 1 \end{bmatrix}$$
$$\mathbf{C_{T_{22}}} = [0 \quad 1], \mathbf{D_{T_{22}}} = [0].$$

By checking the above outlined conditions it can be shown that $\Sigma_{T_{11}}$, though being neither controllable nor observable, it is both stabilizable and detectable. On the contrary, $\Sigma_{T_{22}}$ is neither stabilizable nor detectable. Thus, for the port-pair (2,2) the MIMO system $\Sigma_T$ features *unstable port-level hidden dynamics*, while for the port-pair (1,1) though present, the *port-level hidden dynamics* is not unstable. Accordingly, the stability of the MIMO system $\Sigma_T$ can be accurately predicted by evaluating poles of $T_{11}(s) = \frac{1}{s-1}$, but not by evaluating poles of $T_{22}(s) = \frac{1}{s+3}$. Thus, without prior knowledge on whether (and for which port-pair) the considered MIMO system $\Sigma_T$ features *unstable port-level hidden dynamics*, both[14] $T_{11}(s)$ and $T_{22}(s)$ must be evaluated to accurately determine (BIBO) stability of $\Sigma_T$.

## REFERENCES


[1] D. Boroyevich, I. Cvetkovic, D. Dong, R. Burgos, and F. Lee, "Future electronic power distribution systems - a contemplative view," in *Proc. Int. Conf. Optimisation Elect. Electron. Equip.*, 2010, pp. 1369–1380.

[2] A. Riccobono and E. Santi, "Comprehensive review of stability criteria for DC power distribution systems," in *Proc. IEEE Energy Convers. Congr. Expos.*, 2012, pp. 3917–3925.

[3] P. Pan et al., "An impedance-based stability assessment methodology for DC distribution power system with multi-voltage levels," *IEEE Trans. Power Electron.*, vol. 35, no. 4, pp. 4033–4047, Apr. 2020.

[4] M. Leng, G. Zhou, H. Li, G. Xu, F. Blaabjerg, and T. Dragicevic, "Impedance-based stability evaluation for multibus DC microgrid without constraints on subsystems," *IEEE Trans. Power Electron.*, vol. 37, no. 1, pp. 932–943, Jan. 2021.

[5] M. Amin and M. Molinas, "Small-signal stability assessment of power electronics based power systems: A discussion of impedance- and eigenvalue-based methods," *IEEE Trans. Ind. Appl.*, vol. 53, pp. 5014–5030, Sep./Oct. 2017.

[6] I. Cvetkovic, Z. Liu, D. Boroyevich, and R. Burgos, "On-line measurement of inward and outward impedances for stability assessment," in *Proc. IEEE Electric Ship Technol. Symp.*, 2019, pp. 113–118.

[7] B. Wen, D. Boroyevich, R. Burgos, P. Mattavelli, and Z. Shen, "Inverse nyquist stability criterion for grid-tied inverters," *IEEE Trans. Power Electron.*, vol. 32, no. 2, pp. 1548–1556, Feb. 2017.

[8] J. Sun, "Two-port characterization and transfer immittances of AC-DC converters Part II: Applications," *IEEE Open J. Power Electron.*, vol. 2, pp. 483–510, 2021, doi: 10.1109/OJPEL.2021.3104496.

[9] J. Sun, "Two-port characterization and transfer immittances of AC-DC converters Part I: Modeling," *IEEE Open J. Power Electron.*, vol. 2, pp. 440–462, 2021, doi: 10.1109/OJPEL.2021.3104502.

[10] R. Middlebrook, "Input filter considerations in design and application of switching regulators," *IEEE Industry Appl. Soc. Annu. Meeting*, Chicago, IL, pp. 366–382, Oct. 1976.


[14] In a general case of a nondiagonal $\mathbf{T}(s)$, stability of also all non-diagonal elements of $\mathbf{T}(s)$ must be evaluated to accurately determine stability of $\mathbf{T}(s)$, as elaborated in Section III-B.

[11] H. Y. Cho and E. Santi, "Modeling and stability analysis of cascaded multi-converter systems including feedforward and feedback control," in *Poc. IEEE Ind. Appl. Soc. Annu. Meeting*, 2008, pp. 1–8.
[12] I. Z. Petric, P. Mattavelli, and S. Buso, "Passivation of grid-following VSCs: A comparison between active damping and multi-sampled PWM," *IEEE Trans. Power Electron.*, vol. 37, no. 11, pp. 13205–13216, Nov. 2022.
[13] R. Cvetanovic, I. Z. Petric, P. Mattavelli, and S. Buso, "Accurate high-frequency modeling of the input admittance of PWM grid-connected VSCs," *IEEE Trans. Power Electron.*, vol. 37, no. 9, pp. 10534–10545, Sep. 2022.
[14] I. Z. Petric, P. Mattavelli, and S. Buso, "Multi-sampled grid-connected VSCs: A path toward inherent admittance passivity," *IEEE Trans. Power Electron.*, vol. 37, no. 7, pp. 7675–7687, Jul. 2022.
[15] Y. Zhan, X. Xie, and Y. Wang, "Impedance network model based modal observability and controllability analysis for renewable integrated power systems," *IEEE Trans. Power Del.*, vol. 36, no. 4, pp. 2025–2034, Aug. 2021.
[16] M. Belkhayat, "Stability criteria for AC power systems with regulated loads," Ph.D. dissertation, Purdue Univ., 1997.
[17] H. Zong, C. Zhang, X. Cai, and M. Molinas, "Oscillation propagation analysis of hybrid AC/DC grids with high penetration renewables," *IEEE Trans. Power Syst.*, vol. 37, no. 6, pp. 4761–4772, Nov. 2022.
[18] N. Rashidirad, M. Hamzeh, K. Sheshyekani, and E. Afjei, "An effective method for low-frequency oscillations damping in MultiBus DC microgrids," *IEEE Trans. Emerg. Sel. Topics Circuits Syst.*, vol. 7, no. 3, pp. 403–412, Sep. 2017.
[19] I. Cvetkovic, D. Boroyevich, P. Mattavelli, F. Lee, and D. Dong, "Unterminated small-signal behavioral model of DC–DC converters," *IEEE Trans. Power Electron.*, vol. 28, pp. 1870–1879, Apr. 2013.
[20] A. J. Agbemuko, J. L. Domínguez-García, E. Prieto-Araujo, and O. Gomis-Bellmunt, "Dynamic modelling and interaction analysis of multi-terminal VSC-HVDC grids through an impedance-based approach," *Int. J. Elect. Power Energy Syst.*, vol. 113, pp. 874–887, Dec. 2019.
[21] H. Zhang, M. Mehrabankhomartash, M. Saeedifard, Y. Zou, Y. Meng, and X. Wang, "Impedance analysis and stabilization of point-to-point HVDC systems based on a hybrid AC," *IEEE Trans. Ind. Electron.*, vol. 68, no. 4, pp. 3224–3238, Apr. 2021.
[22] H. Zhang, X. Wang, M. Mehrabankhomartash, M. Saeedifard, Y. Meng, and X. Wang, "Harmonic stability assessment of multiterminal DC (MTDC) systems based on the hybrid AC/DC admittance model and determinant-based GNC," *IEEE Trans. Power Electron.*, vol. 37, no. 2, pp. 1653–1665, Feb. 2022.
[23] J. Pedra, L. Sainz, and L. Monjo, "Three-port small signal admittance-based model of VSCs for studies of multi-terminal HVDC hybrid AC/DC transmission grids," *IEEE Trans. Power Syst.*, vol. 36, no. 1, pp. 732–743, Jan. 2021.
[24] S. Skogestad and I. Postlethwaite, *Multivariable Feedback Control: Analysis and Design*. Hoboken, NJ, USA: Wiley, Nov. 2005.
[25] A. G. J. MacFarlane and I. Postlethwaite, "The generalized Nyquist stability criterion and multivariable root loci," *Int. J. Control*, vol. 25, no. 1, pp. 81–127, Jan. 1977.
[26] R. Cvetanovic, I. Petric, P. Mattavelli, and S. Buso, "MIMO analysis of port-coupling induced destabilization of interlinking DC-DC converters," in *Proc. IEEE Appl. Power Electron. Conf. Expo.*, 2024, pp. 2806–2813.
[27] S. Plesnick, J. Berardino, and R. Irwin, "The generalized Nyquist criterion applied to complex DC power system networks," in *Proc. IEEE Electric Ship Technol. Symp.*, 2019, pp. 8–15.
[28] Q. Lin, B. Wen, and R. Burgos, "RHP poles trajectory study for D-Q impedance-based stability monitoring using a power-hardware-in-the-loop testbed," *IEEE Trans. Emerg. Sel. Topics Power Electron.*, vol. 12, no. 2, pp. 1560–1572, Apr. 2024.
[29] R. W. Erickson and D. Maksimović, *Fundamentals of Power Electronics*. Berlin, Germany: Springer Int. Publishing, 2020.
[30] K. Zhou, J. C. Doyle, and K. Glover, *Robust and Optimal Control*. Hoboken, NJ, USA: Prentice Hall, 1996.
[31] P. Seiler, A. Packard, and P. Gahinet, "An introduction to disk margins," *IEEE Control Syst. Mag.*, vol. 40, pp. 78–95, Oct. 2020.
[32] H. Zhang et al., "Loop-at-a-time stability analysis for grid-connected voltage-source converters," *IEEE Trans. Emerg. Sel. Topics Power Electron.*, vol. 9, no. 5, pp. 5807–5821, Oct. 2021.
[33] H. Yu, Y. Wang, H. Zhang, and Z. Chen, "Impedance modeling and stability analysis of triple-active-bridge-converter-based renewable-electricity-hydrogen-integrated metro DC traction power system," *IEEE Trans. Ind. Electron.*, vol. 70, no. 12, pp. 12340–12353, Dec. 2023.
[34] A. MacFarlane and N. Karcanias, "Poles and zeros of linear multivariable systems: A survey of the algebraic, geometric and complex-variable theory," *Int. J.Control*, vol. 24, pp. 33–74, Jul. 1976.

**Ružica Cvetanović** (Graduate Student Member, IEEE) was born in Belgrade, Serbia, in 1996. She received the B.S. and M.S. degrees in electrical engineering from the University of Belgrade, Belgrade, in 2019 and 2020, respectively. Since 2022, she has been working toward the Ph.D. degree in advanced grid-friendly power electronic converters in renewable smart energy systems with the Power Electronics Group, Department of Information Engineering, University of Padova, Padova, Italy.

From 2020 to 2021, she worked with the Power Converters and Systems Group, School of Electrical Engineering, University of Belgrade. In 2021, she joined the Power Electronics Group, Department of Information Engineering, University of Padova, as a Visiting Researcher. Her research interests include modeling and digital control of grid-tied power electronics converters.

**Ivan Z. Petrić** (Member, IEEE) was born in Belgrade, Serbia, in 1994. He received the B.Sc. and M.Sc. degrees in electrical engineering from the University of Belgrade, Serbia, in 2017 and 2018, respectively, and the Ph.D. degree in electrical engineering from the University of Padova, Italy, in 2023.

From 2018 to 2019, he was a Researcher with the Power Electronics, Machines and Control Group, The University of Nottingham, U.K. In 2022, he was a Visiting Researcher with the Electrical Engineering and Computer Sciences Department, University of California, Berkeley, CA, USA. His research interests include modeling and control of power converters, advanced modulation strategies, and grid-connected converters for renewable energy sources and smart microgrids.

**Paolo Mattavelli** (Fellow, IEEE) received the M.S. (Hons.) and Ph.D. degrees in electrical engineering from the University of Padova, Padova, Italy, in 1992 and 1995, respectively.

He is currently a Full Professor in electronics with the University of Padova. His major research interests include analysis, modeling, and control of power converters, grid-connected converters for renewable energy systems and microgrids, and high-temperature and high-power-density power electronics. His current Google Scholar H-index is 81.

Dr. Mattavelli was an Associate Editor for IEEE TRANSACTIONS ON POWER ELECTRONICS from 2003 to 2012. He is a Co-Editor-in-Chief for IEEE TRANSACTIONS ON POWER ELECTRONICS. From 2005 to 2010, he was the Industrial Power Converter Committee Technical Review Chair for IEEE TRANSACTIONS ON INDUSTRY APPLICATIONS. For terms 2003–2006, 2006–2009, and 2013–2015, he was a member-at-large of the IEEE Power Electronics Society's Administrative Committee. He was a recipient of the Prize Paper Award in IEEE TRANSACTIONS ON POWER ELECTRONICS in 2005, 2006, 2011, and 2012, and the 2nd Prize Paper Award at the IEEE Industry Applications Society Annual Meeting in 2007.

**Simone Buso** (Member, IEEE) received the M.Sc. degree in electronic engineering and the Ph.D. degree in industrial electronics from the University of Padova, Italy, in 1992 and 1997, respectively.

He is currently an Associate Professor of electronics with the Department of Information Engineering (DEI), University of Padova. His main research interests are in the industrial and power electronics fields and are related specifically to switching converter topologies, digital control of power converters, renewable energy sources, and smart micro-grids.